Reachback WSN Connectivity: Non-Coherent Zero-Feedback Distributed Beamforming or TDMA Energy Harvesting?

Konstantinos Alexandris, George Sklivanitis, *Student Member, IEEE*, and Aggelos Bletsas, *Senior Member, IEEE*

***Abstract*—This work is motivated by the reachback connectivity scenario in resource-constrained wireless sensor networks (WSNs): a single terminal at maximum power cannot establish a reliable communication link with the intended destination. Thus, neighboring distributed transmitters should contribute their radios and transmission power, in order to achieve reliable transmission of a common message. This work is particularly interested in low-SNR scenarios with unreliable feedback channels, no channel state information (CSI), and commodity radios, where carrier phase/frequency synchronization is not possible. Concrete non-coherent maximum likelihood and energy detection receivers are developed for zero-feedback distributed beamforming. The proposed receivers are compared with non-coherent energy harvesting reception, based on simple time-division multiple access. It is shown that the proposed zero-feedback distributed beamforming receivers overcome connectivity adversities at the low-SNR regime. This is achieved by exploiting signals' alignment of M distributed transmitters (i.e., beamforming), even with commodity radios, at the expense of network (total) power consumption. Application scenarios include resource-constrained WSNs or emergency radio situations.**

***Index Terms*—Non-coherent receivers, reachback connectivity, wireless sensor networks, zero-feedback beamforming.**

I. Introduction

WIRELESS Sensor Networks (WSNs) are typically equipped with low-complexity, battery-operated radios and low-cost isotropic antennas that generate undirected and relatively weak signals. Distributed transmit beamforming (or simply distributed beamforming), i.e., cooperative transmission from two or more distributed terminals, such that the phases of the transmitted signals align and offer a constructive gain towards the intended destination receiver, has been proposed as a means to boost the power of the transmitted signal and improve connectivity in resource-constrained WSNs. Distributed beamforming could in principle offer high directivity, when the network of terminals is designed to operate as a virtual antenna array.

However, several key challenges need to be addressed. Beamforming setups utilize powerful optimization tools [1], [2] that require some type of prior knowledge, either in the form of channel state information (CSI) or its second order statistics, in order to minimize the total transmission power and maximize the received signal-to-noise ratio (SNR). Phase alignment at the receiver depends on carrier and packet synchronization, which play crucial role in the realization of power beamforming gains [3]. However, in distributed (i.e., network) setups, synchronization is quite challenging, since each terminal has its own local oscillator and the network topology is usually unknown. Furthermore, in the case of low SNR scenarios or fast-fading environments where channel estimation often fails but packet-level synchronization is still feasible, non-coherent reception seems an ideal solution.

Several techniques for distributed beamforming have been proposed, including multi-bit (or even single-bit) closed-loop feedback between receiver and distributed transmitters, as described in [4]–[6]. Another approach includes an interference-limited spread-spectrum scheme across the distributed nodes that maintains the beamforming properties of the network [7]. Work in [8] discusses a new timing and phase synchronization method and evaluates its precision in distributed multi-user multiple-input multiple-output (MU-MIMO) setups using wireless open-access research platform (WARP) radios. Phase and time synchronization between the distributed transmitters is achieved with a master-slave setup. Synchronization and signal generation are implemented in a field-programmable-gate-array (FPGA). Moreover, a master-slave architecture for carrier synchronization was investigated in [9]; it was shown that even with phase errors on the order of 60°, SNR gains of 70% are possible. Finally, work in [10] revisits 1-bit feedback distributed beamforming [4] and discusses a scalable synchronization architecture which is based on receiver's wireless feedback and an extended Kalman filter at the transmitters for frequency locking. A proof-of-concept implementation on commercial

Manuscript received July 25, 2013; revised February 2, 2014; accepted May 28, 2014. Date of publication June 12, 2014; date of current version September 8, 2014. This work was supported in part by the European Union (European Social Fund-ESF), and in part by the Greek national funds through the Operational Program "Education and Lifelong Learning" of the National Strategic Reference Framework (NSRF)—Research Funding Program: Thales. Investing in knowledge society through the European Social Fund. The associate editor coordinating the review of this paper and approving it for publication was T. Hou.

K. Alexandris was with the Telecom Laboratory, School of Electronic and Computer Engineering, Technical University of Crete, Chania 73100, Greece. He is now with EURECOM, 06410 Biot, France (e-mail: kalexandris@isc.tuc.gr).

G. Sklivanitis was with the Telecom Laboratory, School of Electronic and Computer Engineering, Technical University of Crete, Chania 73100, Greece. He is now with the Signals, Communications, and Networking Research Group, Department of Electrical Engineering, University at Buffalo, The State University of New York, Buffalo, NY 14260-1920 USA (e-mail: gsklivan@buffalo.edu).

A. Bletsas is with the Telecom Laboratory, School of Electronic and Computer Engineering, Technical University of Crete, Chania 73100, Greece (e-mail: aggelos@telecom.tuc.gr).

Color versions of one or more of the figures in this paper are available online at http://ieeexplore.ieee.org.

Digital Object Identifier 10.1109/TWC.2014.2330295

software-defined radios was also provided. A comprehensive review of distributed beamforming can be found in [11] and references therein. It can be safely said that most prior art on distributed beamforming requires either CSI at the distributed transmitters (e.g., [12]) or feedback (from the receiver) availability or ability to access the transmitter's radio module for carrier phase adjustments.

Furthermore, blind eigenvalue-based detectors exploiting recent random matrix theory [13]–[15] or subspace tracking methods [16], are not always an option, since a significant amount of data (e.g., a large number of transmitted symbols) and increased computational effort are required; such requirements may not be practically feasible in low-complexity, resource-constrained WSN terminals.

Finally, capacity-related results for *centralized* multiple-input multiple-output (MIMO) non-coherent reception in [17], suggest a signal structure through unitary space-time modulation (USTM) [18], [19]. However, such designs are created for centralized multi-antenna transmitters where there are no different carrier frequency offsets (CFOs) among the transmitting elements. Therefore, those structures are not directly applicable to the distributed setup, considered in this work.

In sharp contrast to prior art, this work studies distributed beamforming in a non-traditional fashion, assuming:

- no CSI availability,
- no reliable receiver-based feedback,
- no access to the physical layer for carrier phase adjustments (commodity WSN radio transmitters).

This work is motivated by network partitioning problems, where a network subset is disconnected from the rest of the network, i.e., each terminal alone cannot communicate with a distant receiver, outside its immediate neighborhood (this is also known as the reachback communication scenario). That may occur in resource-constrained WSNs or emergency radio situations, e.g., firefighters' radios that collaborate in order to transmit a common emergency information message outside a burning building.

In such cases, feedback from outside the subset may not be received reliably, while commodity radios, typically utilized in WSNs, may not offer access to the transmitted carrier phase. Work in [20] and [21] showed that zero-feedback beamforming with unsynchronized carriers is possible and provided analysis results in terms of signal alignment probability, signal alignment delay and respective beamforming gains. However, no specific receivers were proposed. Zero-feedback beamforming gains will be offered if the distributed terminals can transmit packets at the same time. Such packet-level simultaneous transmission is possible with a simple protocol, where transmissions are dictated by a master (*maestro*) terminal, at the vicinity of the distributed transmitters, as experimentally shown in [22].

Inability to acquire CSI and establish a reliable feedback channel, both impose significant constraints and offer a challenging problem, that may be initially considered unsolvable: the terminals can either employ zero-feedback distributed beamforming, where each node transmits at maximum power - in which case a concrete receiver is required - or the nodes transmit in a round-robin fashion, i.e., with time-division multiple access (TDMA) (Fig. 1); in the latter case the receiver gathers signal energy from multiple, distributed transmitters (as opposed to single terminal transmission) in order to achieve reliable reception. This work particularly focuses on the low signal-to-noise ratio (SNR) regime and poses the following question: can zero-feedback distributed beamforming outperform TDMA at the low SNR regime, via constructive signal addition with commodity radios, at the expense of total power consumption?

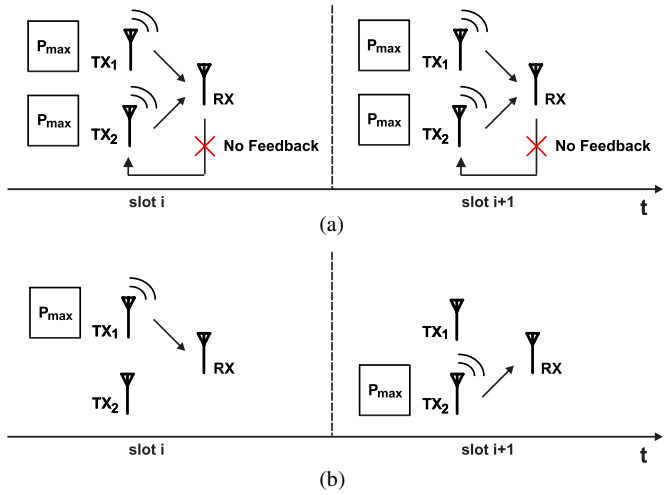

Fig. 1. Transmission schemes. (a) Zero-feedback distributed beamforming. (b) TDMA.

As shown in this work, the answer is positive. Specific non-coherent maximum likelihood and energy detection receivers for the zero-feedback distributed beamforming are presented, and compared with non-coherent energy harvesting (TDMA-based) reception (Fig. 1). Analytical bit error rate (BER) results are also presented. For completeness, USTM is briefly discussed.

Section II introduces the definitions, the basic idea and briefly discusses USTM in the context of distributed transmitters. Section III presents the proposed zero-feedback distributed non-coherent receivers and their BER performance, Section IV provides the TDMA receiver and its BER performance and Section V offers the numerical results. Finally, Section VI concludes this work.

Notation: Upper and lower case bold symbols denote matrices and column vectors, respectively; $\mathbf{I}_N$ denotes the $N \times N$ identity matrix; $0_{N\times N}$ denotes the $N \times N$ zero matrix; $(\cdot)^T$ denotes transpose; $(\cdot)^*$ denotes complex conjugate; $(\cdot)^\dagger$ denotes transpose complex conjugate; $\text{rank}(\mathbf{A})$ denotes the rank of matrix $\mathbf{A}$; $\mathbf{x} \sim \mathcal{CN}(\boldsymbol{\mu}, \boldsymbol{\Sigma})$ denotes that random vector $\mathbf{x}$ is complex Gaussian with mean vector $\boldsymbol{\mu}$ and covariance matrix $\boldsymbol{\Sigma}$[1]; $\mathbf{x} \sim \mathcal{N}(\boldsymbol{\mu}, \boldsymbol{\Sigma})$ denotes that random vector $\mathbf{x}$ is Gaussian with mean vector $\boldsymbol{\mu}$ and covariance matrix $\boldsymbol{\Sigma}$[2]; $\mathcal{G}(k, \theta)$ denotes

[1]The probability density function (p.d.f.) of a N-dimensional $\mathbf{x}$ is given by: $f_{\mathbf{X}}(\mathbf{x}) = \frac{1}{\pi^N \det(\boldsymbol{\Sigma})} \exp\{-(\mathbf{x}-\boldsymbol{\mu})^\dagger \boldsymbol{\Sigma}^{-1}(\mathbf{x}-\boldsymbol{\mu})\}$.

[2]The p.d.f. of a N-dimensional $\mathbf{x}$ is given by: $f_{\mathbf{X}}(\mathbf{x}) = \frac{1}{\sqrt{(2\pi)^N \det(\boldsymbol{\Sigma})}} \exp\{-(1/2)(\mathbf{x}-\boldsymbol{\mu})^T \boldsymbol{\Sigma}^{-1}(\mathbf{x}-\boldsymbol{\mu})\}$.

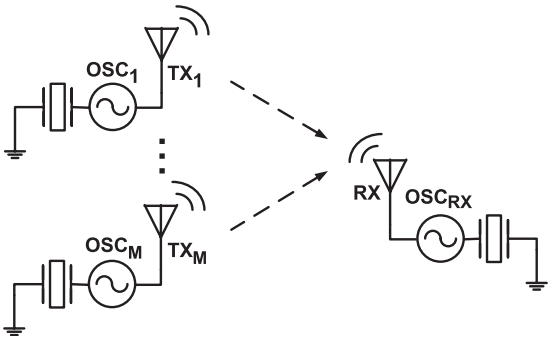

Fig. 2. System setup with M distributed transmitters.

the Gamma distribution with parameters k, θ[3]; erfc$(\cdot)$ stands for the complementary error function[4]; $[a/b]$ stands for the integer division operator; $a \bmod b$ stands for the modulo operator; $a|b$ stands for a divides b i.e., if $a|b$ then $b \bmod a = 0$; $a \nmid b$ stands for a does not divide b ($b \bmod a \neq 0$).

II. System Model and Basic Idea

This work considers M distributed terminals (Fig. 2) that simultaneously transmit a *common* symbol towards a destination terminal at a given frequency band. All M terminals:

- use on-off keying (OOK) modulation, with signal set $\mathcal{X} = \{x_0, x_1\}$, where $x_0 = 0$ and $x_1 = \sqrt{E_1}$;
- operate over Rayleigh, flat-fading channels $h_m \triangleq A_m e^{j\phi_m} \sim \mathcal{CN}(0,1)$, independent across different $m \in \mathcal{T} \triangleq \{1, \ldots, M\}$ (with A_m real and $\phi_m \in [0, 2\pi)$;
- are equipped with non-ideal local oscillators, (i.e., manufacturing inaccuracies result to offsets from the nominal oscillation frequency) thus carrier frequency offsets $\{\Delta f_m\}_{m\in\mathcal{T}}$ are introduced per transmitter-receiver link.

CFO parameters $\{\Delta f_m\}_{m\in\mathcal{T}}$ are assumed to be independent and identically distributed (i.i.d.) random variables according to $\mathcal{N}(0, \sigma_f^2)$. The standard deviation σ_f is set to $\sigma_f = \sqrt{\mathbb{E}[\Delta f_m^2]} = f_c \times \text{ppm}$, where f_c denotes the nominal carrier frequency and ppm denotes the frequency skew of the clock crystals, with typical values of 1–20 parts per million (ppm). Finally, reception of the k^{th} information symbol at the destination occurs in the presence of additive complex white Gaussian noise (CWGN), $w_k \sim \mathcal{CN}(0, \sigma^2)$:

$$y_k \triangleq x_k \sum_{m=1}^{M} h_m e^{+j2\pi\Delta f_m k T_s} + w_k = \widetilde{x}_k + w_k, \qquad (1)$$

where $x_k \in \mathcal{X}$ and $1/T_s$ is the symbol-transmission (baud) rate.

In classic beamforming setups, the transmitted signal per antenna element is multiplied by a complex shaping parameter, such that the aggregate received signal power is strong at a given direction (e.g., towards the destination) and weak towards other directions (hence the term *beamforming*). Inline with the basic assumption of this work that commodity radio modules are assumed, where access to the physical-layer signal is not readily available, the model above does not include the shaping parameters at each transmit antenna. However, the beamforming effect can be achieved with commodity radio due to the constructive addition of multiple signals transmitted by distributed terminals. Specifically, this work exploits the distributed nature of the system setup and particularly the existence of different CFO parameters $\{\Delta f_m\}_{m\in\mathcal{T}}$ per transmitter-receiver link. None of the above holds in the case of a centralized multiple-input single-output system (MISO), where all transmitting antennas share a common oscillator and $\Delta f_m = \Delta f,\ \forall m \in \mathcal{T}$.

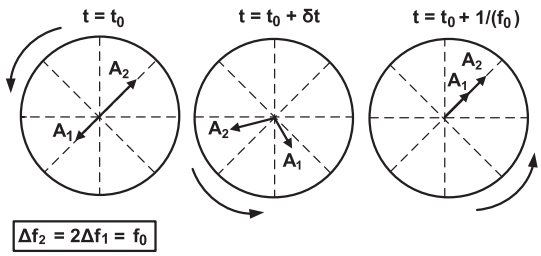

Fig. 3. Zero-feedback distributed beamforming views transmitted signals as rotating phasors with non-zero alignment probability, i.e., there are time instants where signals from distributed transmitters can constructively add.

More specifically, the idea behind zero-feedback distributed beamforming is based on *signal alignment* at the receiver and respective power maximization. The received signal power according to Eq. (1) is given by:

$$\begin{aligned}|\widetilde{x}_k|^2 &= \left| x_k \left(\sum_{m=1}^{M} h_m e^{+j2\pi\Delta f_m k T_s} \right) \right|^2 \\ &= x_k^2 \Bigg\{ \sum_{m=1}^{M} A_m^2 \\ &\quad + 2 \sum_{m\neq i} A_m A_i \cos(2\pi(\Delta f_m - \Delta f_i) k T_s + \phi_m - \phi_i) \Bigg\}. \end{aligned} \qquad (2)$$

The cosine term inside the braces is not necessarily positive, since its value depends on the pairwise CFO and channel phase differences among the different links.

Each transmitted signal $A_m e^{+j(2\pi\Delta f_m k T_s + \phi_m)}$ (see Eq. (1)) can be viewed as a phasor, with angular rotating speed proportional to the respective CFO Δf_m. Thus, there is a non-zero probability that all phasors (signals) align, since they rotate with different angular speeds. For example, consider $M = 2$ distributed transmitters with carrier frequency offsets $\Delta f_2 = 2\Delta f_1 = f_0$ and channel phase difference $\phi_1 - \phi_2 = \pi$ at time instant $t = t_0$, i.e., the two signals add *destructively* at the receiver (Fig. 3). It can be easily seen that at time $t = t_0 + 1/f_0$, the two transmitted signals will be aligned, i.e., they will add *constructively*, offering beamforming gain, provided that the same information symbol is repetitively transmitted by both transmitters and the wireless channel fading parameters remain constant; in other words, a zero-feedback distributed setup can create an alignment event that offers beamforming gain,

[3]The p.d.f. is given by: $f_X(x;k,\theta) = \frac{1}{\theta^k} \cdot \frac{1}{\Gamma(k)} \cdot x^{k-1} \cdot e^{-\frac{x}{\theta}} \cdot u(x)$, where $u(\cdot)$ denotes the unit step function and $\Gamma(k) = (k-1)!$ for any positive integer.

[4]The error complementary function is given by: $\text{erfc}(x) = \frac{2}{\sqrt{\pi}} \int_x^{+\infty} e^{-t^2} dt$.

even with commodity radios (hence the term zero-feedback distributed beamforming).

In [20] the authors analytically calculated the alignment probability as a function of time, for M signals/phasors within a sector of angle ϕ_0, discussed the expected number of symbols where alignment occurs, the required average length of repetition and studied the feasibility of such schemes. It was shown that such steady-state alignment probability depends on the repetition length and not on the clock frequency skew (in ppm) or the wireless channel's phase offsets $\{\phi_m\}_{m\in\mathcal{T}}$, sparking interest on research for non-coherent reception. Frequency skew (in ppm) only affects how fast steady-state alignment probability will be achieved [20]. Non-coherent reception is ideal for low SNR scenarios or fast-fading environments where channel estimation often fails but packet-level synchronization is still feasible. This work extends zero-feedback distributed beamforming proposed in [20], by offering concrete, non-coherent receivers.

Parameter L denotes the number of transmitted symbols per block (block-length). The term "phase" used in this work describes the duration of L symbols after which a new phase begins and the fading coefficients are changed independently from the previous ones (quasi-static fading). CFO parameters are assumed random but constant, during one phase.[5] Finally, it is assumed that $L\cdot\sigma_f\cdot T_s \ll 1$, since L must be kept low (so that $1/L$ is large, as will be further explained below), while $\sigma_f\cdot T_s$ is significantly smaller than unity for typical values. For instance, for $L=3$, crystals of 2 ppm (2×10^{-6}) and binary modulation rate of 1 Mbps at 2.4 GHz, $L\cdot\sigma_f\cdot T_s = 0.0144 \ll 1$. This assumption will be relaxed in the analysis and numerical results sections.

Moreover, the average SNR per m^{th} transmitter antenna per k^{th} time slot is defined as:

$$\text{SNR} \triangleq \frac{\mathbb{E}\left[x_k^2\right]}{\mathbb{E}\left[|w_k|^2\right]} = \frac{E_1}{2\sigma^2}. \tag{3}$$

It is noted that when the transmitters are allowed to simultaneously transmit different symbols, the resulting scheme corresponds to distributed space-time coding, fundamentally different than the beamforming setup of this work. Work in [19] studied the problem of non-coherent reception in classic MIMO systems with unitary space-time modulation; due to the co-located setup, different CFOs among different links were naturally not incorporated in their model. Given that the MIMO design in [18] is non-coherent, we study for completeness its MISO special case, in the context of distributed terminals, where CFO parameters $\{\Delta f_m\}_{m\in\mathcal{T}}$ are prominent. The Rayleigh fading coefficients are assumed to be constant for T symbols and CWGN is added at the receiver. For a single receiver and M transmitting antennas, the model in [18] simplifies to a $\widetilde{\mathbf{y}}$ vector of length-T, where its t^{th} element is given by:

$$\widetilde{y}_t = \sqrt{\frac{\rho}{M}}\sum_{m=1}^{M} h_m e^{+j2\pi\Delta f_m t T_s} s_{tm} + w_t, \tag{4}$$

[5]CFO typically changes with temperature; the latter can be assumed constant for a number of transmitted bits.

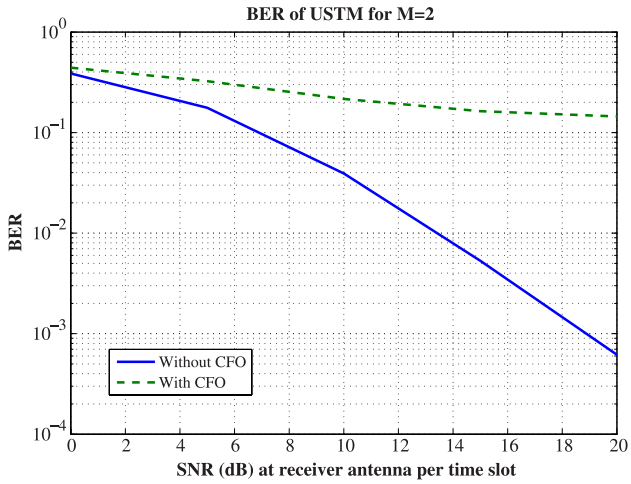

Fig. 4. Simulation BER performance using USTM for $M=2$, $T=8$ and $R=1$ bit/symbol, for the conventional, centralized (CFO-free) and distributed (CFO-limited) case (as in this work).

for $t\in\{1,\ldots,T\}$. Coefficient ρ represents the expected SNR at the receiver antenna and s_{tm} stands for the $(t,m)^{\text{th}}$ element of the $T\times M$ space-time matrix $\mathbf{S}$. The systematic design of $\mathbf{S}$ is presented in [19].

The existence of CFOs and the distributed counterpart vastly changes the design requirements. Fig. 4 depicts BER performance of USTM, for the cases with and without CFOs; constellation of $2^{R\times T}$ signals was assumed, with $R=1$ bit/symbol and $T=8$. The unitary space-time signals were constructed for $M=2$ transmitting antennas, $K=1$ (dimension of the block code), $q=257$ (arithmetic base [19, Table I]). The SNR at the single receiving antenna per time slot is ρ [19, Eq. (1)]. Without CFOs, USTM achieves reduced BER, while for the distributed case (i.e., presence of $\{\Delta f_m\}_{m\in\mathcal{T}}$), performance is degraded, as expected, since USTM has been designed for the centralized, CFO-free MIMO case.

Therefore, different non-coherent transmission schemes (including the USTM methodology) need to be devised for the distributed setup. From that perspective, the distributed zero-feedback beamforming receivers of this work target a newly formulated problem, which could be of potential academic and industry interest.

III. Distributed Transmit Beamforming Receivers

Repetitive transmission exploits signal alignment event, as explained above. The M distributed transmitters simultaneously transmit the same information symbol for L slots, while the channel values remain unchanged (Fig. 5). The achieved rate is $1/L$ and according to the system assumptions, the binary hypothesis test is given by:

$$\begin{aligned} H_0 &: \mathbf{y} = \mathbf{w}, \\ H_1 &: \mathbf{y} = \mathbf{g}x_1 + \mathbf{w}, \end{aligned} \tag{5}$$

where

$$\mathbf{g} \triangleq [g_1 \ \cdots \ g_l \ \cdots \ g_L]^T, \tag{6}$$

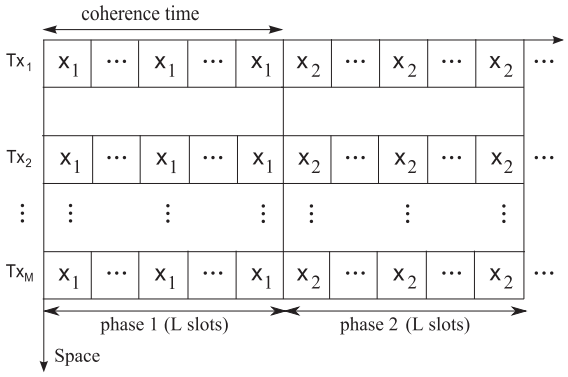

Fig. 5. Repetitive transmission scheme. The M distributed transmitters simultaneously transmit the same information symbol for L slots, while the channel parameters remain unchanged.

and

$$\mathbf{w} \triangleq [w_1 \ \cdots \ w_l \ \cdots \ w_L]^T. \tag{7}$$

The random variable $g_l \triangleq \sum_{m=1}^{M} h_m e^{+j2\pi\Delta f_m l T_s}, \ \forall l \in \{1, 2, \ldots, L\}$, is proved to be distributed according to $\mathcal{CN}(0, M)$ (see Appendix A, Lemma 1). The noise vector elements are i.i.d. according to $w_l \sim \mathcal{CN}(0, \sigma^2)$ for $l \in \{1, \ldots, L\}$.

This scheme is used both in Section III-A and B for the derived detectors.

A. Heuristic Detector

The slots, where signal alignment occurs, are not *a priori* known. Thus, a subset of slots cannot be pre-selected for detection but instead all L symbols are taken into account, using a square-law technique:

$$\mathbf{y}^\dagger \mathbf{y} = \sum_{l=1}^{L} |y_l|^2. \tag{8}$$

Under H_0, the squared $\mathcal{L}_2$ norm of $\mathbf{y}$ is a Gamma-distributed random variable, as a sum of i.i.d. exponentials:

$$H_0 : \mathbf{y}^\dagger \mathbf{y} = \sum_{l=1}^{L} |w_l|^2 \triangleq w \sim \mathcal{G}(L, \sigma^2). \tag{9}$$

Under H_1 and given $\{\Delta f_m\}_{m\in\mathcal{T}}$, the squared $\mathcal{L}_2$ norm of $\mathbf{y}$, is a sum of correlated, identically Gamma-distributed random variables, i.e.,

$$H_1 | \{\Delta f_m\}_{m\in\mathcal{T}} : \quad \mathbf{y}^\dagger \mathbf{y} = \sum_{l=1}^{L} |y_l|^2 = \sum_{l=1}^{L} \zeta_l, \zeta_l \sim \mathcal{G}\left(1, M x_1^2 + \sigma^2\right), \tag{10}$$

and ρ_{ij} is the correlation coefficient between ζ_i and ζ_j

$$\rho_{ij} = \frac{\mathrm{cov}[\zeta_i, \zeta_j]}{\sqrt{\mathrm{var}[\zeta_i]\mathrm{var}[\zeta_j]}}, i \neq j, i, j \in \{1, 2, \ldots, L\} = \frac{x_1^4 \left\{ M + 2\sum_{k\neq n} \cos\left[2\pi T_s (\Delta f_k - \Delta f_n)(i-j)\right] \right\}}{\left(M x_1^2 + \sigma^2\right)^2}. \tag{11}$$

The sum in the ρ_{ij} calculation above is performed over all $\binom{M}{2}$ possible CFO pairs $(\Delta f_k, \Delta f_n)$, for $k, n \in \mathcal{T}$.

A closed form for the p.d.f. of the sum of correlated Gamma is provided in [23, Eq. (5)] while in [24], is offered as a function of the $L \times L$ matrix $\mathbf{K}$,

$$\mathbf{K} = \begin{bmatrix} 1 & \sqrt{\rho_{12}} & \cdots & \sqrt{\rho_{1L}} \\ \sqrt{\rho_{21}} & 1 & \cdots & \sqrt{\rho_{2L}} \\ \vdots & & & \cdots \\ \sqrt{\rho_{L1}} & \sqrt{\rho_{L2}} & \cdots & 1 \end{bmatrix}, \tag{12}$$

for the special case where $\mathbf{K}$ is positive definite and $\rho_{ij} > 0$. In our problem, $\mathbf{K}$ is not necessarily positive definite and ρ_{ij} may be negative. Thus, relevant analytical results in [23] and [24] are not applicable in this work.

Instead, the detection threshold of the binary test is calculated with a heuristic method, taking advantage of the known statistics under H_0. The non-coherent heuristic detector is given by:

$$\mathbf{y}^\dagger \mathbf{y} = \sum_{l=1}^{L} |y_l|^2 \overset{H_1}{\geq} \theta_1(k). \tag{13}$$

In order to estimate an appropriate value for threshold θ_1, the probability of error under H_0, $P(e|H_0)$, is considered, i.e., the error of deciding that $x_1 = \sqrt{E_1}$ was transmitted instead of the correct $x_0 = 0$. The considered threshold is given by:

$$\theta_1(k) = \mathbb{E}[w] + k\sqrt{\mathrm{var}[w]} = \sigma^2[L + k\sqrt{L}], k > 0, \tag{14}$$

where k is a positive parameter selected through simulations, in order to minimize the probability of error and random variable w was defined in Eq. (9). An upper bound of parameter k is acquired by calculating the probability of error under H_0 as follows:

$$P(e|H_0) \leq \epsilon \Leftrightarrow \frac{1}{(L-1)!}\Gamma\left(L, \frac{\theta_1(k)}{\sigma^2}\right) \leq \epsilon, \tag{15}$$

where for example $\epsilon = 10^{-6}$ and $\Gamma(a, z) = \Gamma(a) - \gamma(a, z) = \int_z^{+\infty} t^{a-1} e^{-t} dt; \Re(a) > 0$, $\gamma(a, z)$ is the incomplete Gamma function [25, p. 260, Eq. (6.5.2)] and $\Gamma(a)$ is the Gamma function [25, p. 255, Eq. (6.1.1)]. Such k from Eq. (15) is only an *upper* bound and does not optimize the overall BER, since $P(e|H_1)$ is not taken into account. Near-optimal k will be found through simulations, such that both $P(e|H_1)$ and $P(e|H_0)$ are considered.

B. Maximum-Likelihood Non-Coherent Detector for Fully-Correlated Equivalent Channel Taps

The maximum-likelihood detector derived in this paragraph is based on fully-correlated[6] *equivalent channel taps*[7] $\{\widetilde{g}_l\}_{l=1}^{L} = \sqrt{\frac{1}{M}}\{g_l\}_{l=1}^{L}$.

[6]The elements of a vector $\mathbf{x} = [x_1 \ x_2 \ \ldots \ x_N]^T$ are fully-correlated, if the correlation coefficient $\rho_{x_i x_j} = 1, \ \forall i, j \in \{1, 2, \ldots, N\}$.

[7]At this point and throughout this paper, the term "equivalent channel taps" will stand for $\{\widetilde{g}_l\}_{l=1}^{L}$.

Theorem 1: The random vector $\mathbf{g}$ is distributed according to $\mathcal{CN}(\mathbf{0}, \boldsymbol{\alpha}\boldsymbol{\alpha}^{\dagger}M)$, where $\boldsymbol{\alpha}=[1\ \cdots\ 1]^T$, if $L\cdot\sigma_f\cdot T_s\simeq 0$ (in the sense of $e^{-2[\pi(k-l)\sigma_f T_s]^2}\simeq 1$ for $k\neq l, k, l\in\{1,2,\ldots,L\}$).

Proof: The random vector $\widetilde{\mathbf{g}}$ is defined as $\widetilde{\mathbf{g}}\triangleq\sqrt{\frac{1}{M}}\mathbf{g}$, where

$$\widetilde{\mathbf{g}}=[\widetilde{g}_1\ \cdots\ \widetilde{g}_l\ \cdots\ \widetilde{g}_L]^T,\quad l\in\{1,2,\ldots,L\},\tag{16}$$

and random variable $\widetilde{g}_l=\sqrt{\frac{1}{M}}\sum_{m=1}^{M}h_m e^{+j2\pi\Delta f_m l T_s}\sim\mathcal{CN}(0,1)$. For notational convenience, random vectors

$$\mathbf{h}\triangleq[h_1\ \cdots\ h_M]^T,\tag{17}$$

and

$$\mathbf{e}\triangleq[\Delta f_1\ \cdots\ \Delta f_M]^T,\tag{18}$$

are defined. The random variables $\{\widetilde{g}_l\}_{l=1}^{L}$ are correlated and their $L\times L$ covariance matrix is expressed as $\mathbf{C}=\mathbb{E}[\widetilde{\mathbf{g}}\widetilde{\mathbf{g}}^{\dagger}]$. The $(k,l)^{\text{th}}$ element of covariance matrix $\mathbf{C}$, for $k, l\in\{1,\cdots,L\}$, is analytically computed as follows:

$$\begin{aligned}
&\mathbb{E}_{\mathbf{h},\mathbf{e}}\left[\widetilde{g}_k\widetilde{g}_l^*\right]\\
&=\mathbb{E}_{\mathbf{h},\mathbf{e}}\left[\left(\sqrt{\frac{1}{M}}\sum_{m=1}^{M}h_m e^{+j2\pi\Delta f_m k T_s}\right)\right.\\
&\qquad\left.\times\left(\sqrt{\frac{1}{M}}\sum_{n=1}^{M}h_n e^{+j2\pi\Delta f_n l T_s}\right)^*\right]\\
&=\frac{1}{M}\sum_{m=1}^{M}\mathbb{E}_{\mathbf{h},\mathbf{e}}\left[|h_m|^2 e^{+j2\pi\Delta f_m(k-l)T_s}\right]\\
&\overset{h_m,\Delta f_m}{\underset{\text{indep.}}{=}}\frac{1}{M}\sum_{m=1}^{M}\mathbb{E}_{h_m}\left[|h_m|^2\right]\mathbb{E}_{\Delta f_m}\left[e^{+j2\pi\Delta f_m(k-l)T_s}\right]\\
&=\frac{1}{M\sqrt{2\pi\sigma_f^2}}\sum_{m=1}^{M}\int_{-\infty}^{+\infty}e^{\frac{+j4\pi\sigma_f^2\Delta f_m(k-l)T_s-\Delta f_m^2}{2\sigma_f^2}}d\Delta f_m.
\end{aligned}\tag{19}$$

The integral above in Eq. (19) is computed according to [26, p. 163. Eq. (7.7.6)]:

$$\begin{aligned}
I&=\lim_{x\to-\infty}\left[\int_{x}^{+\infty}e^{\frac{+j4\pi\sigma_f^2\Delta f_m(k-l)T_s-\Delta f_m^2}{2\sigma_f^2}}d\Delta f_m\right]\\
&=\frac{1}{2}\sqrt{2\pi\sigma_f^2}e^{-2[\pi(k-l)\sigma_f T_s]^2}\\
&\quad\times\lim_{x\to-\infty}\operatorname{erfc}\left(\sqrt{\frac{1}{2\sigma_f^2}}x-j\sqrt{2}\pi(k-l)\sigma_f T_s\right)\\
&=\sqrt{2\pi\sigma_f^2}e^{-2[\pi(k-l)\sigma_f T_s]^2}.
\end{aligned}\tag{20}$$

From Eqs. (19), (20), the $(k,l)^{\text{th}}$ element of covariance matrix $\mathbf{C}$ becomes:

$$\mathbb{E}_{\mathbf{h},\mathbf{e}}\left[\widetilde{g}_k\widetilde{g}_l^*\right]=e^{-2[\pi(k-l)\sigma_f T_s]^2},\tag{21}$$

and the matrix $\mathbf{C}$ is analytically described as:

$$\begin{aligned}
\mathbf{C}&=\mathbb{E}[\widetilde{\mathbf{g}}\widetilde{\mathbf{g}}^{\dagger}]\\
&=\begin{bmatrix}1&\cdots&e^{-2[\pi(1-L)\sigma_f T_s]^2}\\ \vdots&\ddots&\vdots\\ e^{-2[\pi(L-1)\sigma_f T_s]^2}&\cdots&1\end{bmatrix}.
\end{aligned}\tag{22}$$

Note that the $(k,l)^{\text{th}}$ element of matrix $\mathbf{C}$, $e^{-2[\pi(k-l)\sigma_f T_s]^2}\simeq 1$, for $k\neq l$, if the exponent $-2[\pi(k-l)\sigma_f T_s]^2\simeq 0$. A sufficient condition for the above approximation is $L\cdot\sigma_f\cdot T_s\simeq 0$. The square included in the exponent accelerates convergence of the exponential term to unity, when the sufficient condition $L\cdot\sigma_f\cdot T_s\simeq 0$ is satisfied. In that case, all the elements of random vector $\widetilde{\mathbf{g}}$ are fully-correlated (in the sense of $e^{-2[\pi(k-l)\sigma_f T_s]^2}\simeq 1$ for $k\neq l, k, l\in\{1,2,\ldots,L\}$), since their correlation coefficient $\rho_{\widetilde{g}_k\widetilde{g}_l}\simeq 1$, for $k\neq l$. Considering this case, the random vector $\widetilde{\mathbf{g}}$ can be replaced by the random vector $\boldsymbol{\alpha}g_0\sim\mathcal{CN}(\mathbf{0},\boldsymbol{\alpha}\boldsymbol{\alpha}^{\dagger})$, where $g_0\sim\mathcal{CN}(0,1)$ and $\boldsymbol{\alpha}=[1\ \cdots\ 1]^T$. Exploiting the above, it can be directly concluded that $\mathbf{g}$ is distributed according to $\mathcal{CN}(\mathbf{0},\boldsymbol{\alpha}\boldsymbol{\alpha}^{\dagger}M)$. ■

Corollary 1: For the case of fully-correlated *equivalent channel taps* $\{\widetilde{g}_l\}_{l=1}^{L}$ (in the sense of $e^{-2[\pi(k-l)\sigma_f T_s]^2}\simeq 1$ for $k\neq l, k, l\in\{1,2,\ldots,L\}$), $\mathbf{g}$ is distributed according to $\mathcal{CN}(\mathbf{0},\boldsymbol{\alpha}\boldsymbol{\alpha}^{\dagger}M)$.

In many real-world WSNs scenarios, the condition $L\cdot\sigma_f\cdot T_s\simeq 0$ is satisfied. For instance, if $\sigma_f=2.4$ GHz $\times$ 2 ppm $=$ 4.8 kHz, $T_s=1$ μs (i.e., rate 1 Mbps for binary modulation) and $L=4$, then $e^{-2[\pi(k-l)\sigma_f T_s]^2}\simeq 1$, for $k\neq l$. This is a frequent case, assuming high transmission rate in RF bands and a typical value of 2 ppm (2×10^{-6}) for clock crystals and small L for repetitive transmission in order to avoid rate degradation.

Using Corollary 1 and under hypothesis $H_1:\mathbf{y}\sim\mathcal{CN}(\mathbf{0},\boldsymbol{\alpha}\boldsymbol{\alpha}^{\dagger}Mx_1^2+\sigma^2\mathbf{I}_L)$, as an affine transformation of independent circularly-symmetric complex Gaussian random vectors and under $H_0:\mathbf{y}\sim\mathcal{CN}(\mathbf{0},\sigma^2\mathbf{I}_L)$. The non-coherent ML receiver, assuming equiprobable symbols, is described by the following expression:

$$f_{\mathbf{y}|H_1}\overset{H_1}{\geq}f_{\mathbf{y}|H_0},\tag{23}$$

which is simplified to the following expression:

$$\mathbf{y}^{\dagger}\mathbf{D}\mathbf{y}\overset{H_1}{\geq}\theta_2\triangleq\sigma^2\ln\left[\det\left(\mathbf{I}_L+\boldsymbol{\alpha}\boldsymbol{\alpha}^{\dagger}\frac{Mx_1^2}{\sigma^2}\right)\right],\tag{24}$$

where $\mathbf{D}\triangleq\mathbf{I}_L-\left(\mathbf{I}_L+\boldsymbol{\alpha}\boldsymbol{\alpha}^{\dagger}(Mx_1^2/\sigma^2)\right)^{-1}$.

It is noted that for not fully-correlated equivalent channel taps $\{\widetilde{g}_l\}_{l=1}^{L}$, the p.d.f. of $\mathbf{g}$ is not known. Given $\{\Delta f_m\}_{m\in\mathcal{T}}$, the random vector $\mathbf{g}$ can be written as:

$$\mathbf{g}=\mathbf{A}\mathbf{h},\tag{25}$$

where $\mathbf{h}$ is given from Eq. (17) and the $L\times M$ matrix $\mathbf{A}$ is given by:

$$\mathbf{A}=\begin{bmatrix}e^{+j2\pi\Delta f_1 T_s}&\cdots&e^{+j2\pi\Delta f_M T_s}\\ \vdots&\ddots&\vdots\\ e^{+j2\pi\Delta f_1 L T_s}&\cdots&e^{+j2\pi\Delta f_M L T_s}\end{bmatrix}.\tag{26}$$

Consequently, given the CFOs, $\mathbf{g}$ is distributed according to the conditional p.d.f. $f_{\mathbf{g}|\mathbf{A}}(\mathbf{g}|\mathbf{A}) = f_{\mathbf{g}|\{\Delta f_m\}_{m\in\mathcal{T}}}(\mathbf{g}|\{\Delta f_m\}_{m\in\mathcal{T}}) \equiv \mathcal{CN}(\mathbf{0}, \mathbf{A}\mathbf{A}^\dagger)$, as a linear combination of a circularly-symmetric complex Gaussian vector $\mathbf{h} \sim \mathcal{CN}(\mathbf{0}, \mathbf{I}_M)$. However, the p.d.f. of $\mathbf{A}$ is not known, and thus, a closed form for the unconditioned p.d.f. of $\mathbf{g}$ cannot be derived.

Therefore, for partially correlated and uncorrelated equivalent channel taps, a heuristic receiver is proposed by replacing the term $\boldsymbol{\alpha}\boldsymbol{\alpha}^\dagger$ of Eq. (24) with $\mathbf{C}$:

$$\mathbf{y}^\dagger \mathbf{G} \mathbf{y} \overset{H_1}{\geq} \theta_3 \triangleq \sigma^2 \ln \left[\det \left(\mathbf{I}_L + \mathbf{C} \frac{M x_1^2}{\sigma^2} \right) \right], \tag{27}$$

where $\mathbf{C}$ is given by Eq. (22) and $\mathbf{G} \triangleq \mathbf{I}_L - (\mathbf{I}_L + \mathbf{C}(M x_1^2/\sigma^2))^{-1}$.

1) BER Performance Analysis:

Theorem 2: Assuming fully-correlated equivalent channel taps and equiprobable hypotheses, the average BER for the ML non-coherent detector is given by:

$$P(e) = \frac{1}{2} \left[1 - F_r\left(\boldsymbol{\lambda}_{H_0}, \theta_2\right) + F_r\left(\boldsymbol{\lambda}_{H_1}, \theta_2\right) \right], \tag{28}$$

where under hypothesis H_i, $i \in \{0, 1\}$, $F_r(\boldsymbol{\lambda}_{H_i}, \theta_2)$ is the CDF of $\mathbf{y}^\dagger \mathbf{D} \mathbf{y}$. Furthermore, analytical form of CDF $F_r(\boldsymbol{\lambda}_{H_i}, \theta_2)$ is given in Appendix B. Vector $\boldsymbol{\lambda}_{H_i}$ contains the eigenvalues of a $2L \times 2L$ matrix $(\boldsymbol{\Sigma}_{H_i})^{1/2} \mathbf{E} (\boldsymbol{\Sigma}_{H_i})^{1/2}$, $r = \text{rank}(\mathbf{E})$, $\mathbf{E} = \begin{bmatrix} \mathbf{D} & 0_{L\times L} \\ 0_{L\times L} & \mathbf{D} \end{bmatrix}$, $\boldsymbol{\Sigma}_{H_0} = \begin{bmatrix} (1/2)\sigma^2 \mathbf{I}_L & 0_{L\times L} \\ 0_{L\times L} & (1/2)\sigma^2 \mathbf{I}_L \end{bmatrix}$ and $\boldsymbol{\Sigma}_{H_1} = \begin{bmatrix} (1/2)(\boldsymbol{\alpha}\boldsymbol{\alpha}^\dagger M x_1^2 + \sigma^2 \mathbf{I}_L) & 0_{L\times L} \\ 0_{L\times L} & (1/2)(\boldsymbol{\alpha}\boldsymbol{\alpha}^\dagger M x_1^2 + \sigma^2 \mathbf{I}_L) \end{bmatrix}$.

Proof: Assuming equipropable hypotheses, BER is written as:

$$\begin{aligned} P(e) &= \sum_{i=0}^{1} P(e|H_i) P(H_i) \\ &= \frac{1}{2} \left[P(\mathbf{y}^\dagger \mathbf{D} \mathbf{y} \geq \theta_2 | H_0) + P(\mathbf{y}^\dagger \mathbf{D} \mathbf{y} < \theta_2 | H_1) \right], \end{aligned} \tag{29}$$

where $P(e|H_i)$ for $i = 0, 1$ are calculated by the CDF of $\mathbf{y}^\dagger \mathbf{D} \mathbf{y}$ described in Appendix B-Eq. (37). ■

IV. Non-Coherent Energy Harvesting (TDMA) Receiver

A time-slotted protocol among M distributed terminals is used to schedule transmission to the intended destination. M distributed terminals transmit the same symbol using time-division multiplexing for L slots (one phase). Each distributed terminal transmits separately from the others the same symbol for $[L/M]$ slots. In that way, the receiver augments the received energy, in order to reliably detect each information symbol at the expense of transmission rate. If M does not divide L ($M \nmid L$), the remaining slots are allocated to the m^{th} terminal, that is selected randomly (uniformly) (Fig. 6). Assuming CFO correction at the receiver, the signal model is expressed as:

$$\mathbf{y} = \widetilde{\mathbf{h}} x + \mathbf{w}, \tag{30}$$

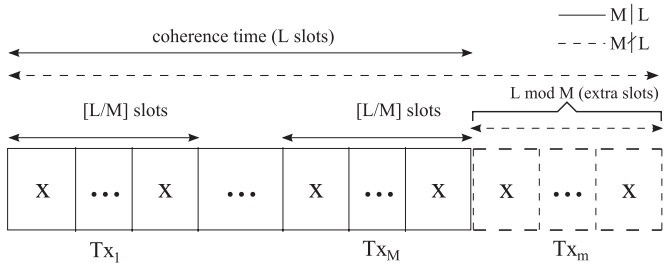

Fig. 6. Non-coherent energy harvesting (TDMA) scheme.

where $\widetilde{\mathbf{h}} = [\underbrace{h_1 \cdots h_1}_{[L/M]} \ \cdots \ \underbrace{h_M \cdots h_M}_{[L/M]}]^T$, if $M|L$ and $\widetilde{\mathbf{h}} = [\underbrace{h_1 \cdots h_1}_{[L/M]} \ \cdots \ \underbrace{h_M \cdots h_M}_{[L/M]} \ \underbrace{h_m \cdots h_m}_{L \bmod M}]^T$, if $M \nmid L$. Finally, random variable $h_m \sim \mathcal{CN}(0, 1), m \in \{1, \ldots, M\}$ and random vector $\mathbf{w} \sim \mathcal{CN}(\mathbf{0}, \mathbf{I}_L)$.

A. Maximum-Likelihood Non-Coherent Detector

Given the hypotheses, Eq. (30) can be written as:

$$\begin{aligned} H_0 &: \mathbf{y} = \mathbf{w}, \\ H_1 &: \mathbf{y} = \mathbf{B}\mathbf{h} x_1 + \mathbf{w}, \end{aligned} \tag{31}$$

where

$$\mathbf{B} = \begin{bmatrix} 1 & 0 & \cdots & 0 & 0 \\ & & \vdots & & \\ 1 & 0 & \cdots & 0 & 0 \\ 0 & 1 & \cdots & 0 & 0 \\ & & \vdots & & \\ 0 & 1 & \cdots & 0 & 0 \\ & & \vdots & & \\ 0 & 0 & \cdots & 0 & 1 \\ & & \vdots & & \\ 0 & 0 & \cdots & 0 & 1 \\ & \text{extra rows} & & & \end{bmatrix} \begin{matrix} \left.\begin{matrix} \\ \\ \end{matrix}\right\} \left[\frac{L}{M}\right] \text{ rows } (1^{\text{st}} \text{ block}) \\ \left.\begin{matrix} \\ \\ \end{matrix}\right\} \left[\frac{L}{M}\right] \text{ rows } (2^{\text{nd}} \text{ block}) \\ \\ \left.\begin{matrix} \\ \\ \end{matrix}\right\} \left[\frac{L}{M}\right] \text{ rows } (M^{\text{th}} \text{ block}) \\ \left.\begin{matrix} \\ \end{matrix}\right\} L \bmod M \text{ rows} \end{matrix}$$

and $\mathbf{h} \sim \mathcal{CN}(\mathbf{0}, \mathbf{I}_M)$ according to Eq. (17).

Each block of $[L/M]$ rows of matrix $\mathbf{B}$ corresponds to the m^{th} user transmission. If $M \nmid L$, then the extra rows of matrix $\mathbf{B}$ are selected to be the same with one of the $[L/M]$ rows of the m^{th} user block. Thus, the extra rows correspond to a different m^{th} user which is selected uniformly.

Under $H_1 : \mathbf{y} \sim \mathcal{CN}(\mathbf{0}, \mathbf{B}\mathbf{B}^\dagger x_1^2 + \sigma^2 \mathbf{I}_L)$ as an affine transformation of independent circularly-symmetric complex Gaussian random vectors and under $H_0 : \mathbf{y} \sim \mathcal{CN}(\mathbf{0}, \sigma^2 \mathbf{I}_L)$. Similarly to the zero-feedback distributed beamforming scheme, by assuming equiprobable symbols, the non-coherent

receiver is based on the maximum-likelihood method (see Eq. (23)) and is given by:

$$\mathbf{y}^{\dagger}\mathbf{R}\mathbf{y} \overset{H_1}{\geq} \Theta \triangleq \sigma^2 \ln\left[\det\left(\mathbf{I}_L + \mathbf{B}\mathbf{B}^{\dagger}\frac{x_1^2}{\sigma^2}\right)\right], \quad (32)$$

where $\mathbf{R} \triangleq \mathbf{I}_L - (\mathbf{I}_L + \mathbf{B}\mathbf{B}^{\dagger}(x_1^2/\sigma^2))^{-1}$.

1) BER Performance: Using the methodology in Section III-B1, the CDF of complex quadratic form $\mathbf{y}^{\dagger}\mathbf{R}\mathbf{y}$ is needed to describe the probability of error under each hypothesis. The theorem below provides BER analysis of the TDMA receiver both for the case of $M|L$ and $M\nmid L$.

Theorem 3: Assuming equiprobable symbols, BER closed form both for the cases of $M|L$ and $M\nmid L$ is given by:

$$P(e) = \begin{cases} \frac{1}{2}\left[1 - F_r\left(\boldsymbol{\lambda}_{H_0}, \Theta\right) + F_r\left(\boldsymbol{\lambda}_{H_1}, \Theta\right)\right], & \text{if } M|L, \\ \frac{1}{2M}\sum_{j=1}^{M}\left[1 - F_r\left(\boldsymbol{\lambda}_{H_0}^{j}, \Theta\right) + F_r\left(\boldsymbol{\lambda}_{H_1}^{j}, \Theta\right)\right], & \text{if } M\nmid L, \end{cases} \quad (33)$$

where $F_r(\cdot,\cdot)$ is, the CDF of $\mathbf{y}^{\dagger}\mathbf{R}\mathbf{y}$ (given at the Appendix B). $\mathbf{E} = \begin{bmatrix} \mathbf{R} & 0_{L\times L} \\ 0_{L\times L} & \mathbf{R} \end{bmatrix}$, $\boldsymbol{\Sigma}_{H_0} = \begin{bmatrix} (1/2)\sigma^2\mathbf{I}_L & 0_{L\times L} \\ 0_{L\times L} & (1/2)\sigma^2\mathbf{I}_L \end{bmatrix}$ and $\boldsymbol{\Sigma}_{H_1} = \begin{bmatrix} (1/2)(\mathbf{B}\mathbf{B}^{\dagger}x_1^2 + \sigma^2\mathbf{I}_L) & 0_{L\times L} \\ 0_{L\times L} & (1/2)(\mathbf{B}\mathbf{B}^{\dagger}x_1^2 + \sigma^2\mathbf{I}_L) \end{bmatrix}$. Under hypothesis H_i, $i \in \{0,1\}$, vectors $\boldsymbol{\lambda}_{H_i}$ (case for $M|L$) and $\boldsymbol{\lambda}_{H_i}^{j}$ (case for $M\nmid L$) contain the eigenvalues of the $2L \times 2L$ matrix $(\boldsymbol{\Sigma}_{H_i})^{1/2}\mathbf{E}(\boldsymbol{\Sigma}_{H_i})^{1/2}$, where for the case of $M|L$, matrix $\mathbf{E}$ is based on $\mathbf{R}$ constructed by $\mathbf{B}$ without including any extra rows and for the case of $M\nmid L$, matrix $\mathbf{E}$ is based on $\mathbf{R}$ constructed by $\mathbf{B}$ with extra rows (i.e., the $L \bmod M$ rows of the j^{th} user block). Finally, $r = \text{rank}(\mathbf{E})$.

Proof: Considering the cases of $M|L$, $M\nmid L$ and assuming equiprobable symbols, the analysis follows as:
If $M|L$, BER is computed as:

$$P(e) = \sum_{i=0}^{1} P(e|H_i)P(H_i) = \frac{1}{2}\sum_{i=0}^{1} P(e|H_i)$$

$$= \frac{1}{2}\left[P(\mathbf{y}^{\dagger}\mathbf{R}\mathbf{y} \geq \Theta|H_0) + P(\mathbf{y}^{\dagger}\mathbf{R}\mathbf{y} < \Theta|H_1)\right]. \quad (34)$$

If $M\nmid L$, BER is computed as:

$$P(e) = \frac{1}{2}\sum_{i=0}^{1} P(e|H_i) = \frac{1}{2}\sum_{j=1}^{M}\sum_{i=0}^{1} P(e \cap \text{Tx}_j|H_i)$$

$$= \frac{1}{2}\sum_{j=1}^{M}\sum_{i=0}^{1} P(e|\text{Tx}_j, H_i)\underbrace{P(\text{Tx}_j|H_i)}_{P(\text{Tx}_j)}, \quad (35)$$

where Tx_j denotes the event of the j^{th} user transmission at the extra allocated slots. Since the extra slots are allocated uniformly, the probability $P(\text{Tx}_j)$ is set to $P(\text{Tx}_j) = \frac{1}{M}$. Consequently, Eq. (35) becomes:

$$P(e) = \frac{1}{2M}\sum_{j=1}^{M}\sum_{i=0}^{1} P(e|\text{Tx}_j, H_i)$$

$$= \frac{1}{2M}\sum_{j=1}^{M}\left[P(e|\text{Tx}_j, H_0) + P(e|\text{Tx}_j, H_1)\right]$$

$$= \frac{1}{2M}\sum_{j=1}^{M}\left[P(\mathbf{y}^{\dagger}\mathbf{R}\mathbf{y} \geq \Theta|\text{Tx}_j, H_0)\right.$$

$$\left. + P(\mathbf{y}^{\dagger}\mathbf{R}\mathbf{y} < \Theta|\text{Tx}_j, H_1)\right]. \quad (36)$$

Using the derived closed form CDF of $\mathbf{y}^{\dagger}\mathbf{R}\mathbf{y}$, as described in Appendix B-Eq. (37), under each hypothesis and given the j^{th} user transmission (implying $\mathbf{R}$ construction with extra rows in $\mathbf{B}$, the $L \bmod M$ rows of the j^{th} user block, if $M\nmid L$ or no extra rows if $M|L$), Eq. (34) and Eq. (36) result in Eq. (33).

Parameter r is the same for both the cases of $M|L$ and $M\nmid L$, since for the case of $M\nmid L$, the addition of extra rows in matrix $\mathbf{B}$ leaves the rank of matrix $\mathbf{B}$ unchanged and thus the rank of matrix $\mathbf{R}$ is also the same. ■

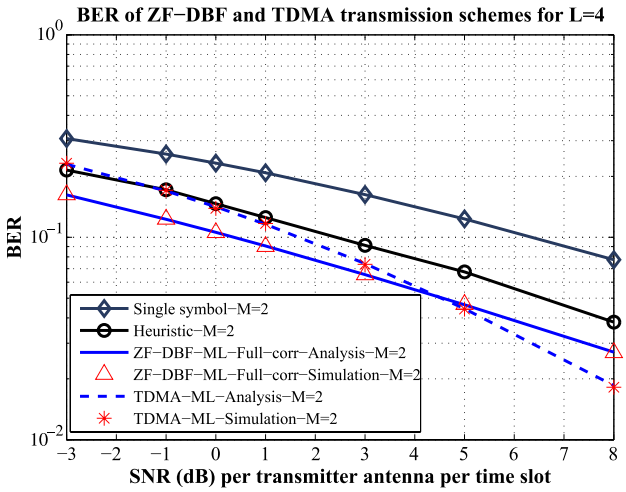

Fig. 7. BER performance for ZF-DBF and TDMA transmission schemes ($L = 4$).

V. Numerical Results

Both simulation and analytical BER results are presented with SNR per transmitter antenna per time slot, as defined in Eq. (3), $f_c = 2.4$ GHz, $T_s = 1$ μs (i.e., 1 Mbps) and 2 ppm (2×10^{-6}) clock crystals. For these values, the received samples at the destination receiver are fully-correlated and exploited in the appropriate detector (Figs. 7–10). Block-length parameter L was kept relatively small (on the order of 3–4), so that rate degradation $1/L$ was also kept small. Therefore, blind eigenvalue-based detectors are not comparable, since they require large block-length.

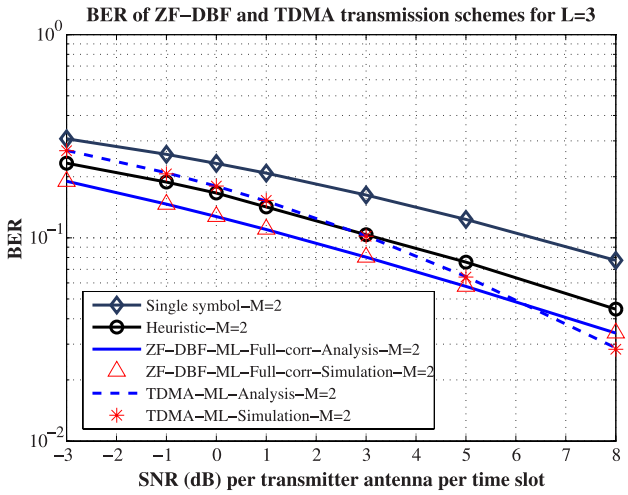

Fig. 8. BER performance for ZF-DBF and TDMA transmission schemes ($L = 3$).

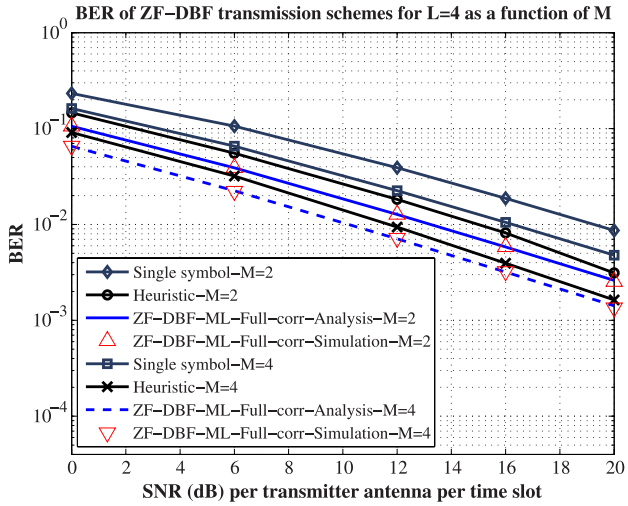

Fig. 9. BER performance for ZF-DBF transmission schemes with different number of M distributed terminals.

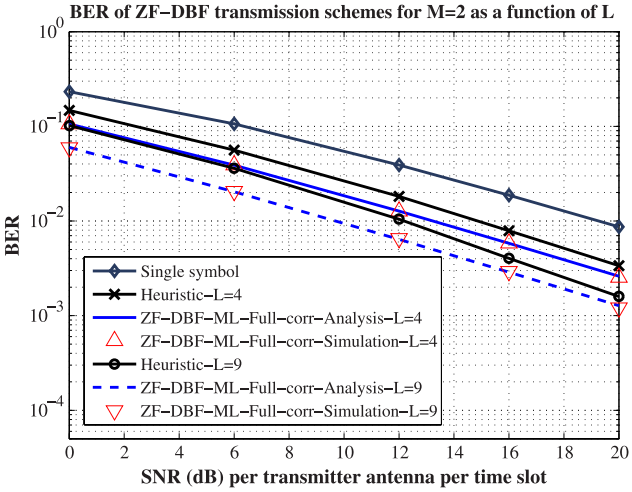

Fig. 10. BER performance for ZF-DBF transmission schemes in different L time intervals.

Fig. 7 shows BER as a function of SNR per transmitter antenna per time slot for the zero-feedback distributed beamforming (ZF-DBF) and the energy harvesting (TDMA) scheme, $M = 2$ distributed transmitters and $L = 4$ symbols. It is shown that analysis and simulation results agree. The ZF-DBF ML receiver based on fully-correlated equivalent channel taps results in better performance than the heuristic receiver, as expected. Furthermore, the ZF-DBF ML receiver for fully-correlated equivalent channel taps outperforms the TDMA receiver for SNR values up to 5 dB. Better performance at lower SNR of ZF-DBF is due to its beamforming gain, at the expense of total additional transmission power (by a factor of M for each slot), compared to TDMA. The latter performs better at higher SNR due to the diversity offered by the M independent transmitter-receiver channels. For comparison reference purposes, BER performance for single symbol non-coherent detector (ZF-DBF ML detector of Eq. (24) for $L = 1$) is also depicted.

Fig. 8 demonstrates BER simulation and analytical results for the ZF-DBF and TDMA schemes, $M = 2$ distributed transmitters and smaller L value ($L = 3$ symbols). For the case of ZF-DBF receivers, the expected number of symbols (out of $L = 4$) with $M = 2$ aligned signals within at most $\phi_0 = \pi/4$ is 1, assuming that out of this sector ϕ_0, the signals are not considered aligned. This implies that there is one slot on average with beamforming gain in $L = 4$ time slots. In other words, the minimum repetitive transmission length L should be selected in order to guarantee signal alignment during at least one slot out of L. For $L = 3$, the expected number of symbol slots with signal alignment can be easily obtained using [20, Eq. (12)] and is strictly smaller than 1. Thus, by reducing the number of slots to $L = 3$, the achieved rate $(1/L)$ is increased, however alignment is not guaranteed and BER performance is degraded, as Fig. 8 depicts. Furthermore, for $L = 3$ the ZF-DBF receiver outperforms TDMA for SNR values smaller than 6 dB; TDMA performance is degraded by 1 dB compared to $L = 4$, since less slots reduce the effects of diversity. On the other hand, smaller L improves rate. Thus, for all schemes, there is a trade-off between better rate and reliable communication, with ZF-DBF offering smaller BER (and thus better reachback connectivity) at lower SNR, at the expense of total transmission power. However, in reachback connectivity scenarios, using the battery of the neighboring terminal for distributed transmission may be the only valid option.

Fig. 9 provides simulation and analytical BER results for the ZF-DBF scheme for $L = 4$ symbols and different number of M distributed terminals. For larger values of M, signal alignment occurs with smaller probability, which decreases exponentially with M [20]; BER is reduced with increasing number of transmitters, at the expense of total transmission power; again, trading total (network) transmission power with connectivity (and respective communication reliability) is preferable in reachback connectivity scenarios; in those cases one node transmitting alone at maximum power does not suffice; instead, zero-feedback beamforming could be employed, where the unconnected distributed transmitters could contribute their radios and transmission power.

Fig. 10 depicts BER performance for the ZF-DBF scheme for a different number of symbols L and $M = 2$ distributed

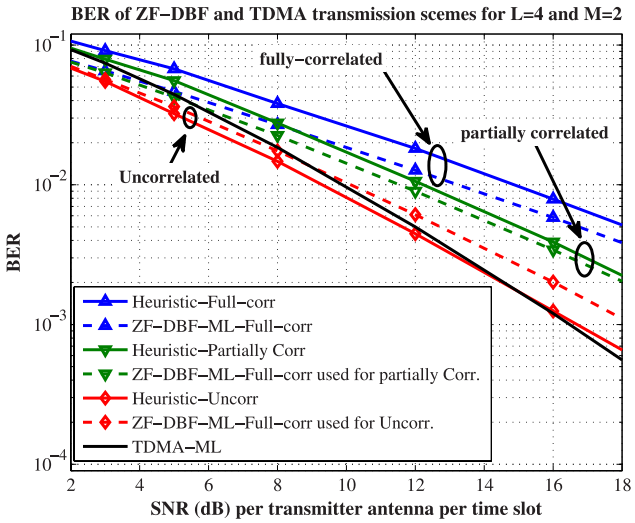

Fig. 11. BER performance for ZF-DBF and TDMA transmission schemes including different cases of equivalent channel taps correlation.

terminals. It can be easily seen that as L increases, BER performance is also improved, since more transmissions of the same information symbol offers reliability, at the expense of total power consumption and rate degradation.

Fig. 11 presents BER performance for different cases of equivalent channel taps correlation. Both partially correlated equivalent channel taps with $T_s = 1$ μs, 20 ppm (20×10^{-6}) clock crystals and uncorrelated equivalent channel taps with $T_s = 0.4$ ms, 2 ppm (2×10^{-6}) clock crystals are considered. The selection of these parameters results in a different covariance matrix $\mathbf{C}$ (see Eq. (22)). Fully-correlated equivalent channel taps offer a matrix $\mathbf{C}$ of ones, uncorrelated equivalent channel taps create a matrix $\mathbf{C}$ equal to the identity matrix and partially correlated equivalent channel taps provide a matrix $\mathbf{C}$ with elements valued between 0 and 1. Fig. 11 depicts the ZF-DBF detector (described in Eq. (24) and Eq. (27) respectively) for all the equivalent channel taps correlation types. Furthermore, TDMA receiver BER performance provided, is the same for all correlation cases, since it is independent of $\{\Delta f_m\}_{m\in\mathcal{T}}$ due to coarse and fine CFO correction conducted at the receiver. Both for the heuristic and ZF-DBF receiver, partially correlated and uncorrelated equivalent channel taps offer better BER performance compared to the fully-correlated case, since instantaneous deep fading or signals destructive addition does not affect all the received samples. ZF-DBF receiver is optimal only for the case of fully-correlated equivalent channel taps, thus heuristic receiver performs better for the uncorrelated equivalent channel taps. On the other hand, it is noted that for partially correlated equivalent channel taps, ZF-DBF still dominates the latter. Finally, the heuristic receiver for the uncorrelated equivalent channel taps outperforms all the other schemes, at the low SNR regime, alleviating the reachback communication problem.

VI. Conclusion

This work has presented concrete non-coherent receivers for zero-feedback distributed beamforming and compared them with non-coherent detection of a TDMA-based scheme. It was motivated by resource-constrained WSNs, where one node transmitting at maximum power cannot reliably communicate with the intended far-reaching destination, as in reachback connectivity problems. Moreover, it was shown that the proposed zero-feedback distributed beamforming receivers overcome connectivity adversities, at the low-SNR regime. This is achieved by exploiting signals' alignment of M distributed transmitters (i.e., beamforming), at the expense of network (total) power consumption. No (transmitter or receiver) CSI, no receiver feedback for carrier/phase synchronization and only commodity radio hardware were assumed, in sharp contrast to prior art. On the other hand in high SNR cases, where connectivity is not an issue and one node is used per time slot, TDMA outperforms the other schemes and ensures reliability due to multi-user diversity. Finally, a discussion of USTM schemes with and without CFO was also offered, pointing towards new research directions.

Appendix A
PDF of the Complex Random Variable g_l

Lemma 1: The random variable $g_l \triangleq \sum_{m=1}^{M} h_m e^{+j2\pi\Delta f_m l T_s}$, $\forall l \in \{1, 2, \ldots, L\}$, is distributed according to $\mathcal{CN}(0, M)$.

Proof: Given $\{\Delta f_m\}_{m\in\mathcal{T}}$, $g_l \sim \mathcal{CN}(0, M)$ as a linear combination of circularly-symmetric complex Gaussian random variables $\{h_m\}_{m\in\mathcal{T}} \sim \mathcal{CN}(0, 1)$. Thus, $f_{g_l|\{\Delta f_m\}_{m\in\mathcal{T}}}(g_l|\{\Delta f_m\}_{m\in\mathcal{T}}) \equiv \mathcal{CN}(0, M)$, which is independent of CFOs $\{\Delta f_m\}_{m\in\mathcal{T}}$. By taking the expectation over $\{\Delta f_m\}_{m\in\mathcal{T}}$, the PDF of g_l is given by:

$$f_{g_l}(g_l) = \mathbb{E}_{\mathbf{e}}\left[f_{g_l|\mathbf{e}}(g_l|\mathbf{e})\right] = f_{g_l|\mathbf{e}}(g_l|\mathbf{e}) \int_{-\infty}^{+\infty} f_{\mathbf{e}}(\mathbf{e})\, d\mathbf{e}$$

$$= f_{g_l|\mathbf{e}}(g_l|\mathbf{e}),$$

where $\mathbf{e} = [\Delta f_1 \ \ldots \ \Delta f_M]^T$. ■

Appendix B
CDF of a Complex Quadratic Form $\mathbf{y}^\dagger \boldsymbol{\mathcal{A}} \mathbf{y}$

Lemma 2: Let $\mathbf{y}^\dagger \boldsymbol{\mathcal{A}} \mathbf{y}$ the complex quadratic form of $L \times 1$ $\mathbf{y}$, where $\mathbf{y} \sim \mathcal{CN}(\mathbf{0}, \boldsymbol{\mathcal{C}})$, $\boldsymbol{\mathcal{C}}$ is real, $\boldsymbol{\mathcal{A}}$ is real and $\boldsymbol{\mathcal{A}} = \boldsymbol{\mathcal{A}}^T$. Then, the CDF of $\mathbf{y}^\dagger \boldsymbol{\mathcal{A}} \mathbf{y}$ is given by:

$$F_r(\boldsymbol{\lambda}, z) = \sum_{i=0}^{+\infty} (-1)^i c_i \frac{z^{\frac{r}{2}+i}}{\Gamma\left(\frac{r}{2}+i+1\right)}, \tag{37}$$

where $\Gamma(z) = \int_0^{+\infty} t^{z-1} e^{-t} dt$ denotes the Gamma function, vector $\boldsymbol{\lambda} = [\lambda_1 \ \cdots \ \lambda_r]^T$ contains the eigenvalues of $2L \times 2L$ matrix $\boldsymbol{\Sigma}^{1/2}\mathbf{E}\boldsymbol{\Sigma}^{1/2}$, $\boldsymbol{\Sigma} = \begin{bmatrix} \frac{1}{2}\boldsymbol{\mathcal{C}} & 0_{L\times L} \\ 0_{L\times L} & \frac{1}{2}\boldsymbol{\mathcal{C}} \end{bmatrix}$, $\mathbf{E} = \begin{bmatrix} \boldsymbol{\mathcal{A}} & 0_{L\times L} \\ 0_{L\times L} & \boldsymbol{\mathcal{A}} \end{bmatrix}$ and $r = \mathrm{rank}(\mathbf{E})$.

The coefficients $c_i (i \geq 0)$ can be calculated recursively through the relation:

$$c_i \triangleq \begin{cases} \prod_{j=1}^{r} (2\lambda_j)^{-\frac{1}{2}}, & i = 0, \\ \frac{1}{i} \sum_{j=0}^{i-1} d_{i-j} c_j, & i > 0, \end{cases} \tag{38}$$

where $d_i (i \geq 1)$ is expressed as follows:

$$d_i \triangleq \frac{1}{2} \sum_{j=1}^{r} (2\lambda_j)^{-i}, \quad i \geq 1. \tag{39}$$

Proof: Let a complex random vector $\mathbf{y} \sim \mathcal{CN}(\mathbf{0}, \boldsymbol{\mathcal{C}})$. If matrix $\boldsymbol{\mathcal{C}}$ is real, then the real-valued equivalent random vector $\widetilde{\mathbf{y}}$ can be expressed as [27]:

$$\widetilde{\mathbf{y}} \triangleq \left[\Re\{\mathbf{y}\}^T \ \Im\{\mathbf{y}\}^T \right]^T \sim \mathcal{N}(\mathbf{0}, \boldsymbol{\Sigma}), \tag{40}$$

where the real covariance matrix $\boldsymbol{\Sigma} = \begin{bmatrix} \frac{1}{2}\boldsymbol{\mathcal{C}} & 0_{L\times L} \\ 0_{L\times L} & \frac{1}{2}\boldsymbol{\mathcal{C}} \end{bmatrix}$. Define $\mathbf{y}_R \triangleq \Re\{\mathbf{y}\}$, $\mathbf{y}_I \triangleq \Im\{\mathbf{y}\}$ and $\mathbf{E} \triangleq \begin{bmatrix} \boldsymbol{\mathcal{A}} & 0_{L\times L} \\ 0_{L\times L} & \boldsymbol{\mathcal{A}} \end{bmatrix}$, then:

$$\begin{aligned} \mathbf{y}^\dagger \boldsymbol{\mathcal{A}} \mathbf{y} &= \left(\mathbf{y}_R^T - j\mathbf{y}_I^T\right) \boldsymbol{\mathcal{A}} (\mathbf{y}_R + j\mathbf{y}_I) \\ &= \mathbf{y}_R^T \boldsymbol{\mathcal{A}} \mathbf{y}_R + j\mathbf{y}_R^T \boldsymbol{\mathcal{A}} \mathbf{y}_I - j\mathbf{y}_I^T \boldsymbol{\mathcal{A}} \mathbf{y}_R + \mathbf{y}_I^T \boldsymbol{\mathcal{A}} \mathbf{y}_I, \\ \widetilde{\mathbf{y}}^T \mathbf{E} \widetilde{\mathbf{y}} &= \mathbf{y}_R^T \boldsymbol{\mathcal{A}} \mathbf{y}_R + \mathbf{y}_I^T \boldsymbol{\mathcal{A}} \mathbf{y}_I. \end{aligned}$$

Thus, iff $\boldsymbol{\mathcal{A}} = \boldsymbol{\mathcal{A}}^T$, then $\mathbf{y}^\dagger \boldsymbol{\mathcal{A}} \mathbf{y} = \widetilde{\mathbf{y}}^T \mathbf{E} \widetilde{\mathbf{y}}$. Consequently, $\mathbf{y}^\dagger \boldsymbol{\mathcal{A}} \mathbf{y} \equiv \widetilde{\mathbf{y}}^T \mathbf{E} \widetilde{\mathbf{y}}$, and using [28, Theorem 4.2b.1], we conclude in Eq. (37). ■

REFERENCES

[1] N. D. Sidiropoulos, T. N. Davidson, and Z. Q. Luo, "Transmit beamforming for physical layer multicasting," *IEEE Trans. Signal Process.*, vol. 54, no. 6, pp. 2239–2251, Jun. 2006.

[2] V. H. Nassab, S. Shahbazpanahi, A. Grami, and Z. Q. Luo, "Distributed beamforming for relay networks based on second-order statistics of the channel state information," *IEEE Trans. Signal Process.*, vol. 56, no. 9, pp. 4306–4316, Sep. 2008.

[3] S. Song, J. Thompson, P.-J. Chung, and P. Grant, "BER analysis for distributed beamforming with phase errors," *IEEE Trans. Veh. Technol.*, vol. 59, no. 8, pp. 4169–4174, Oct. 2010.

[4] R. Mudumbai, B. Wild, U. Madhow, and K. Ramchandran, "Distributed beamforming using 1 bit feedback: From concept to realization," in *Proc. Allerton Conf. Commun., Control Comput.*, Sep. 2006, pp. 1020–1027.

[5] M. Johnson, K. Ramchandran, and M. Mitzenmacher, "Distributed beamforming with binary signaling," in *Proc. IEEE Int. Symp. Inf. Theory*, Jul. 2008, pp. 890–894.

[6] R. Mudumbai, D. R. Brown, U. Madhow, and H. V. Poor, "Distributed transmit beamforming: Challenges and recent progress," *IEEE Commun. Mag.*, vol. 47, no. 2, pp. 102–110, Feb. 2009.

[7] A. Kalis and A. Kanatas, "Cooperative beamforming in smart dust: Getting rid of multihop communications," *IEEE Pervasive Comput.*, vol. 9, no. 3, pp. 47–53, Jul.–Sep. 2010.

[8] H. Balan, R. Rogalin, A. Michaloliakos, K. Psounis, and G. Caire, "AirSync: Enabling distributed multiuser MIMO with full spatial multiplexing," *IEEE/ACM Trans. on Netw.*, vol. 21, no. 6, pp. 1681–1695, Dec. 2013.

[9] R. Mudumbai, G. Barriac, and U. Madhow, "On the feasibility of distributed beamforming in wireless networks," *IEEE Trans. Wireless Commun.*, vol. 6, no. 5, pp. 1754–1763, May 2007.

[10] F. Quitin, M. Rahman, R. Mudumbai, and U. Madhow, "A scalable architecture for distributed transmit beamforming with commodity radios: Design and proof of concept," *IEEE Trans. Wireless Commun.*, vol. 12, no. 3, pp. 1418–1428, Mar. 2013.

[11] J. Uher, T. Wysocki, and B. Wysocki, "Review of distributed beamforming," *J. Telecommun. Inf. Technol.*, vol. 2011, no. 1, p. 78, Mar. 2011.

[12] Y. Lebrun *et al.*, "Performance analysis of distributed ZF beamforming in the presence of CFO," *EURASIP J. Wireless Commun. Netw.*, vol. 2011, p. 177, Nov. 2011.

[13] S. Chatzinotas, S. K. Sharma, and B. Ottersten, "Asymptotic analysis of eigenvalue-based blind spectrum sensing techniques," in *Proc. IEEE Int. ICASSP*, May 2013, pp. 4464–4468.

[14] Y. Zeng and Y.-C. Liang, "Maximum–minimum eigenvalue detection for cognitive radio," in *Proc. IEEE 18th Int. Symp. PIMRC*, 2007, pp. 1–5.

[15] Y. Zeng and Y.-C. Liang, "Eigenvalue-based spectrum sensing algorithms for cognitive radio," *IEEE Trans. Commun.*, vol. 57, no. 6, pp. 1784–1793, Jun. 2009.

[16] C. G. Tsinos and K. Berberidis, "Adaptive eigenvalue-based spectrum sensing for multi-antenna cognitive radio systems," in *Proc. IEEE ICASSP*, May 2013, pp. 4454–4458.

[17] T. L. Marzetta and B. M. Hochwald, "Capacity of a mobile multiple-antenna communication link in Rayleigh flat fading," *IEEE Trans. Inf. Theory*, vol. 45, pp. 139–157, Jan. 1993.

[18] B. M. Hochwald and T. L. Marzetta, "Unitary space-time modulation for multiple-antenna communication in Rayleigh flat-fading," *IEEE Trans. Inf. Theory*, vol. 46, pp. 543–564, Mar. 2000.

[19] B. Hochwald, T. Marzetta, T. Richardson, W. Sweldens, and R. Urbanke, "Systematic design of unitary space-time constellations," *IEEE Trans. Inf. Theory*, vol. 46, no. 6, pp. 1962–1973, Sep. 2000.

[20] A. Bletsas, A. Lippman, and J. Sahalos, "Simple, zero-feedback, distributed beamforming with unsynchronized carriers," *IEEE J. Sel. Areas Commun.*, vol. 28, no. 7, pp. 1046–1054, Sep. 2010.

[21] A. Bletsas, A. Lippman, and J. Sahalos, "Zero-feedback, collaborative beamforming for emergency radio: Asymptotic analysis," *Mobile Netw. Appl. (MONET)*, vol. 16, no. 5, pp. 589–599, Oct. 2011.

[22] G. Sklivanitis, K. Alexandris, and A. Bletsas, "Testbed for non-coherent zero-feedback distributed beamforming," in *Proc. IEEE ICASSP*, May 2013, pp. 2563–2567.

[23] M. S. Alouini, A. Abdi, and M. Kaveh, "Sum of gamma variates and performance of wireless communication systems over Nakagami-fading channels," *IEEE Trans. Veh. Technol.*, vol. 50, no. 6, pp. 1471–1480, Nov. 2001.

[24] J. F. Paris, A Note on the Sum of Correlated Gamma Random Variables, Mar. 2011. [Online]. Available: http://arXiv.org/abs/1103.0505

[25] M. Abramowitz and I. A. Stegun, *Handbook of Mathematical Functions With Formulas, Graphs, Mathematical Tables*. New York, NY, USA: Dover, 1964.

[26] F. W. Olver, D. W. Lozier, R. F. Boisvert, and C. W. Clark, *NIST Handbook of Mathematical Functions*, 1st ed. New York, NY, USA: Cambridge Univ. Press, 2010.

[27] R. Gallager, Circularly-Symmetric Gaussian Random Vectors, Jan. 2008. [Online]. Available: http://www.rle.mit.edu/rgallager/documents/CircSymGauss.pdf

[28] A. Mathai and S. Provost, *Quadratic Forms in Random Variables: Theory and Applications*. New York, NY, USA: Marcel Dekker, 1992, ser. Statistics: A Series of Textbooks and Monographs.

Konstantinos Alexandris received the Diploma and M.Sc. degrees (with distinction) in electronic and computer engineering from the Technical University of Crete, Chania, Greece, in 2012 and 2014, respectively. He was with the Telecommunications Circuits Laboratory (TCL), École Polytechnique Fédérale de Lausanne, Switzerland, as a Research Assistant for eight months. He is currently working toward the Ph.D. degree with the Mobile Communications Department, EURECOM, Biot, France. His research interests are in the areas of wireless cellular networks, wireless communications, wireless sensor networks, software-defined radio implementations, and software-defined networking. He has received fellowship awards for his undergraduate studies. He was the recipient of the 2011–2012 Best Diploma Thesis Award on "Advanced Wireless Systems," presented by the IEEE Vehicular Technology Society and Aerospace and Electronic Systems Society joint Greece Chapter.

George Sklivanitis (S'11) received his Diploma in electronic and computer engineering from the Technical University of Crete, Chania, Greece, in 2010. He is currently working toward the Ph.D. degree in electrical engineering at the University at Buffalo, The State University of New York, and is a Research Assistant with the Signals, Communications and Networking Research Group. His research interests are in the area of wireless communications, signal processing, and wireless networking with an emphasis on real-time adaptive signal processing, massive MIMO communications, cognitive radio, software-defined radio networks, and underwater acoustic communications. He is a Student Member of the IEEE Communications and Signal Processing Societies. He was the winner of the 2014 Nutaq Software-Defined Radio Academic US National Contest.

Aggelos Bletsas (S'03–M'05–SM'14) received the Diploma degree (with excellence) in electrical and computer engineering from Aristotle University of Thessaloniki, Thessaloniki, Greece, in 1998 and the S.M. and Ph.D. degrees from the Massachusetts Institute of Technology, Cambridge, MA, USA, in 2001 and 2005, respectively. He was at Mitsubishi Electric Research Laboratories, Cambridge, as a Postdoctoral Fellow and at Radiocommunications Laboratory, Department of Physics, Aristotle University of Thessaloniki, as a Visiting Scientist. He joined the School of Electronic and Computer Engineering, Technical University of Crete, in the summer of 2009, as an Assistant Professor and was promoted to Associate Professor at the beginning of 2014. His research interests span the broad area of scalable wireless communication and networking, with emphasis on relay techniques, backscatter communications and RFID, energy harvesting, radio hardware/software implementations for wireless transceivers, and low cost sensor networks. His current vision and focus is on single-transistor front-ends and backscatter sensor networks, for large-scale environmental sensing. He is the Principal Investigator of project "BLASE: Backscatter Sensor Networks for Large-Scale Environmental Sensing," funded by the General Secretariat of Research and Technology Action "Proposals evaluated positively from the 3rd European Research Council (ERC) Call." He is also a Management Committee Member and a National Representative in the European Union COST Action IC1301 "Wireless Power Transmission for Sustainable Electronics (WiPE)." He is an Associate Editor of the IEEE WIRELESS COMMUNICATIONS LETTERS since its foundation and a Technical Program Committee Member of flagship IEEE conferences. He holds two patents from USPTO and he was recently included in http://www.highlycitedgreekscientists.org/. He was the corecipient of the IEEE Communications Society 2008 Marconi Prize Paper Award in Wireless Communications, Best Paper Distinction at ISWCS 2009, Siena, Italy, Second Best Student Paper Award at the IEEE RFID-TA 2011, Sitges, Barcelona, Spain and Best Paper distinction at IEEE Sensors Conf. 2013, Baltimore, MD, USA. Two of his undergraduate advisees were winners of the 2009–2011 and 2011–2012 Best Diploma Thesis Contest, respectively, among all Greek Universities on "Advanced Wireless Systems," awarded by IEEE VTS/AES joint Greek Chapter. At the end of 2013, he was awarded the Technical University of Crete 2013 Research Excellence Award.